Journal of Applied Physics

Layer specific optical band gap measurement at nanoscale in MoS_2 and ReS_2 van der Waals compounds by high resolution electron energy loss spectroscopy

Cite as: J. Appl. Phys. **119**, 114309 (2016); https://doi.org/10.1063/1.4944431
Submitted: 14 January 2016 . Accepted: 05 March 2016 . Published Online: 21 March 2016

K. Dileep, R. Sahu, Sumanta Sarkar, Sebastian C. Peter, and R. Datta

JOURNAL OF APPLIED PHYSICS **119**, 114309 (2016)

Layer specific optical band gap measurement at nanoscale in MoS_2 and ReS_2 van der Waals compounds by high resolution electron energy loss spectroscopy

K. Dileep,[1,a)] R. Sahu,[1] Sumanta Sarkar,[2] Sebastian C. Peter,[2] and R. Datta[1,a)]
[1]*International Centre for Materials Science, Chemistry and Physics of Materials Unit, Jawaharlal Nehru Centre for Advanced Scientific Research, Bangalore 560064, India*
[2]*New Chemistry Unit, Jawaharlal Nehru Centre for Advanced Scientific Research, Bangalore 560064, India*

(Received 14 January 2016; accepted 5 March 2016; published online 21 March 2016)

Layer specific direct measurement of optical band gaps of two important van der Waals compounds, MoS_2 and ReS_2, is performed at nanoscale by high resolution electron energy loss spectroscopy. For monolayer MoS_2, the twin excitons (1.8 and 1.95 eV) originating at the K point of the Brillouin zone are observed. An indirect band gap of 1.27 eV is obtained from the multilayer regions. Indirect to direct band gap crossover is observed which is consistent with the previously reported strong photoluminescence from the monolayer MoS_2. For ReS_2, the band gap is direct, and a value of 1.52 and 1.42 eV is obtained for the monolayer and multilayer, respectively. The energy loss function is dominated by features due to high density of states at both the valence and conduction band edges, and the difference in analyzing band gap with respect to ZnO is highlighted. Crystalline 1T ReS_2 forms two dimensional chains like superstructure due to the clustering between four Re atoms. The results demonstrate the power of HREELS technique as a nanoscale optical absorption spectroscopy tool. © *2016 AIP Publishing LLC*.
[http://dx.doi.org/10.1063/1.4944431]

I. INTRODUCTION

Atomically thin monolayer transition metal dichalcogenides (TMDs) are a new class of two dimensional nanomaterial with promising optoelectronic, energy, and novel device applications. One of the important features of many TMDs is that they undergo a crossover from indirect band gap in the bulk to direct band gap in the monolayer form.[1–9] The existence of a direct band gap is a major advantage over graphene for practical device applications. This allows absorbing and emitting light efficiently in the monolayer forms and constructs field effect transistor devices at extremely small length scale.[6,8] The cross over from indirect to direct band gaps has been explained based on strong interlayer coupling and confinement effect.[9] While the monolayer properties of TMDs are unique, it may be illusive while fabricating practical devices. This is because of unavoidable electronic packaging and the property changes in close proximity of foreign substance due to electronic coupling and van der Waals interaction.[10] Therefore, there is an urge to stabilize such novel properties arising from the monolayer in the interface or in the bulk form. With this goal, there is a candidate material already reported in the family, i.e., crystalline 1T-ReS_2, where the interlayer van der Waals coupling is extremely weak, i.e., 18 meV compared to 460 meV of MoS_2.[11] ReS_2 was reported to exhibit monolayer behavior in the bulk form and shows direct band gap in the range of 1.5–1.6 eV. This also offers exploring the 2-D physics of TMDs in 3-D form. Though there are many reports based on this class of materials, so far, mostly photoluminescence technique (with enhanced intensity) combined with first principle based calculation was used to interpret the crossover between indirect to direct band gaps in these systems. To the best of our knowledge, no direct layer specific absorption spectroscopy measurement was ever performed on these systems, nor the details of the optical response was ever studied in terms of energy loss function (ELF). Therefore, we have exploited high resolution electron energy loss spectroscopy (HREELS) to probe layer specific optical band gap in both MoS_2 and ReS_2. The HREELS technique to measure optical band gap is equivalent to optical absorption spectroscopy but with the advantage of selected area information at the nano and atomic scale.[12,13] In addition to this, the high energy electrons (300 kV in the present case) have much larger momentum than equivalent photon and transfer both energy and momentum to the crystal electrons during an inelastic event, thus allowing measurement of both direct and indirect transitions. However, determination of band gap values and their types from the Tauc like plot or the energy loss function have appeared to be complicated in these systems compared to ZnO and previous report[2] because of peaks arising from Van Hove singularities in the density of states (DOS) at near the band edges as well as more than one possible transition within narrow energy range (±0.5 eV). The features in the experimental energy loss function are explained based on calculated DOS and band structure. In MoS_2, an indirect band gap of 1.27 eV and a direct band gap of 1.98 eV are obtained from the multilayer and monolayer, respectively. The twin excitons at 1.8 and 1.95 eV are observed at the onset of direct band gap for the monolayer. In ReS_2, a direct band gap of 1.42 and 1.52 eV are obtained from the

a)Authors to whom correspondence should be addressed. Electronic addresses: dileep@jncasr.ac.in and ranjan@jncasr.ac.in

multilayer and monolayer regions, respectively. High resolution images confirm 2H structure of MoS_2 and a two dimensional Peierls distorted $1T_d$ structure of ReS_2. In case of ReS_2, superstructure along two different directions is observed which is formed due to clustering between four Re atoms, and this is necessary to open a direct band gap else the system would show metallic characteristics. The results demonstrate that HREELS is a powerful technique to measure and identify directly layer specific band gap types in such nanodimensional materials. Moreover, the potential of the technique is enormous particularly after the demonstrations of ~9 meV energy resolution in EELS, which in addition to optical band gaps offers probing the phonon modes at the atomic and nanometer length scale.[14]

II. EXPERIMENTAL DETAILS

TEM samples were prepared by ultra sonication of bulk MoS_2 powder (Sigma Aldrich) and bulk ReS_2 powder followed by drop casting on a holey carbon grid. Rhenium disulfide was synthesized by directly heating small pieces of elemental rhenium cut from a wire (1.0 mm diameter, 99.97%, Alfa Aesar) and sulfur (powder, −325 mesh, 99.5%, Alfa Aesar) in the stoichiometric ratio (1:2) in an evacuated (10^{-5} mbar pressure) quartz tube to 200 °C in 15 h followed by annealing at that temperature for 2 h. This step involving very slow heating to a low temperature was necessary in order to avoid any possibility of explosion due to high vapor pressure of sulfur. Next, the temperature was increased stepwise to 400 °C and finally to 900 °C over the course of 10 and 24 h, respectively. The sample was kept at this temperature for 120 h to ensure proper homogeneity. The final product was a fine black powder.

HRTEM was performed in an aberration corrected FEI TITAN^{3TM} 80–300 kV TEM microscope operating at 300 kV with a negative third order spherical aberration coefficient ($C_s \sim -35\ \mu m$) and a positive defocus value ($\Delta f \sim +8$ nm), which resolve atoms with white contrast in the image.[15,16] Residual aberration was almost the same between the samples given by the corrector software. Exposure time was typically of the order of a second and less, thus beam damage was not apparent. Band gaps and valence electronic structure were determined at the nanoscale using high resolution electron energy loss spectroscopy at 300 kV. A gun monochromator is used which gives energy resolution better than 180 meV as measured from the full width at half maximum (FWHM) of the zero loss peak. The zero loss peaks from the HREELS spectra were removed by fitted logarithm tail method. The Kramers-Kronig analysis was performed to calculate the optical absorption coefficient. The band structure of MoS_2 and ReS_2 shows parabolic dispersion in the k-space, so indirect and direct band gaps can be determined by Tauc plots originally used for amorphous semiconductors like Ge, Si where the "X" intercept of the linear portion of $(\alpha.E)^{0.5}$ vs. E and $(\alpha.E)^2$ vs. E graphs give indirect and direct band gaps, respectively.[17–19] However, this is for ideal parabolic band structure, and the absorption profile may have structures depending on the nature of DOS for a given system. We will see later that the presence of Van Hove singularities in the DOS at the conduction and valence band edges makes application of Tauc like plot extremely difficult. The thickness of the materials under investigation was extremely thin, i.e., monolayer and its multiples depending on the number of layers. Therefore, the effect of Cerenkov radiation on the energy loss spectra was absent.

III. CALCULATION METHODS

Electronic structure calculations were performed using density functional theory (DFT) based on Wien2k code.[20] The code uses linearized augmented plane waves as basis and considers all electrons into the calculation. Following structures were considered for the theoretical calculation: (a) bulk 2H-MoS_2, (b) monolayer 2H-MoS_2, (c) distorted bulk $1T_d$-ReS_2, and (d) distorted monolayer $1T_d$-ReS_2. The schematic of the simulated structures is given in Fig. 1. For bulk 2H-MoS_2 calculation, a unit cell consisting of two MoS_2 formula units with Bernal stacking along the *c*-direction was considered. The dispersion correction due to van der Waals interaction was included according to DFTD3 method.[21] Zero damping method was used in the van der Waals' energy expression. The dispersion interaction was cutoff at 95 bohrs, and the forces were calculated numerically. For monolayer calculation, a vacuum of 16 Å was created between the layers in order to prevent interlayer interactions. Lattice parameters were optimized using Perdew-Burke-Ernzerhof (PBE) functional within generalized gradient approximation (GGA). The convergence criteria for energy and charge were 0.0001 Ry and 0.001 electrons, respectively. The forces were

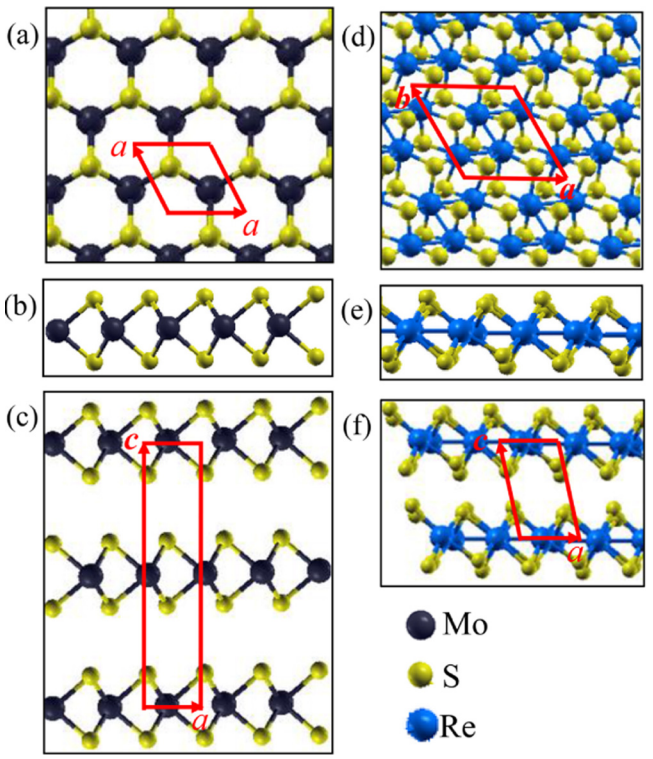

FIG. 1. Schematic structure of (a) monolayer 2H-MoS_2 along ⟨0001⟩, (b) along ⟨11-20⟩, (c) Bernal stacking for bulk 2H-MoS_2 along ⟨11-20⟩, (d) $1T_d$ monolayer ReS_2 along ⟨0001⟩, (e) along ⟨11-20⟩, and (f) Bernal stacking for bulk $1T_d$ along ⟨11-20⟩. Unit cell and in plane lattice vectors are shown. The "N" shaped Re_4 cluster is highlighted.

minimized below 1 mRy/bohr. The relaxed lattice parameters of the bulk MoS_2 are $a = 3.1858$ Å and $c = 12.8540$ Å, respectively. The interlayer distance (the S-S distance) perpendicular to the "c" plane is 3.28 Å. The relaxed a lattice parameter of the monolayer MoS_2 is 3.1917 Å.

A 2×2 superstructure is constructed for the monolayer distorted $1T_d$ ReS_2 where four Re atoms form Re_4 cluster. $1T_d$-ReS_2 is simulated by triclinic unit cell consisting of four ReS_2 units (Fig. 1(f)). The relaxed lattice parameters of the bulk ReS_2 are $a = 6.4112$ Å, $b = 6.4714$ Å, $c = 6.4213$ Å, $\alpha = 91.32°$, $\beta = 105.49°$, and $\gamma = 119.03°$. The interlayer S-S distance in this case is 2.62 Å. The relaxed lattice parameters for monolayer ReS_2 are $a = 6.4308$ Å, $b = 6.4912$ Å, and $\gamma = 119.03°$.

The muffin tin radii R_{MT} were chosen such that they do not overlap. Core and valence states were separated by −6 Ry of energy. The K_{max} value was set to be $7.00/R_{MT\ (min)}$, where $R_{MT\ (min)}$ is the muffin tin radius of the smallest atom, in the present case it is the S atom. A Γ centered $30 \times 30 \times 18$ and $30 \times 30 \times 1$ k-point mesh was used for a unit cell containing two formula units for the bulk and a single formula unit cell for monolayer calculations, respectively, and the number was reduced proportionally for the larger supercell. It is found that only high density k mesh with common multiples of 3 and 2 (6×6, 12×12, etc.) is able to yield correct band gap values from the spin split valence band at K point.

Usually, GGA-PBE underestimates the excited state properties and electronic band gaps significantly for materials with strongly correlated electrons.[22] But in the case of TMX_2 compounds, it gives reasonably good band gaps but can be improved further. Available techniques to correct the excited states, namely, Heyd-Scuseria-Ernzerhof (HSE) functional and GW calculations (G stands for Green function and W stands for Coulomb interaction) are computationally expensive.[23] Instead, we applied a semi-empirical modified Becke–Johnson exchange-correlation potential (known as mBJ potential).[24] This method gives the band gap values close to GW calculations and is computationally fast. The value of the "c" parameter should be properly chosen for accurate determination of the band gap. The "P-semiconductor" scheme was chosen to determine the c-parameter.[25] For MoS_2 and ReS_2, however, mBJGGA does not result in substantial improvement from GGA-PBE band gap value, because it cannot correct when the symmetry of valance band maximum (VBM) and conduction band minimum (CBM) is the same.[26] The CBM and the VBM of MoS_2 are made of Mo d_Z2 orbitals. And, for ReS_2, both VBM and CBM have significant contributions from $d_{x^2-y^2}$ and d_{xy} orbitals.

The linear optical properties for monolayer and bulk MoS_2 and ReS_2 are calculated using OPTIC program in Wien2k.[27] The calculation is also carried out on ZnO to compare the difference between the systems. The momentum matrix elements are calculated with the same dense k-point mesh chosen for the SCF cycles. The imaginary part of the dielectric function is calculated by combining both the momentum matrix elements and the interband transitions summed over the Brillouin zone along different polarization directions. The real part of the dielectric function and energy loss function is then calculated by the Kramers-Kronig transformation. The results obtained from the theoretical calculations are compared with the experimental energy loss functions.

IV. RESULTS AND DISCUSSION

A. High resolution imaging of MoS_2 and ReS_2

HRTEM image of few layers MoS_2 along ⟨0001⟩ Z.A shows the 2H poly-type structure (Fig. 2(a)). Because of the Bernal stacking in few layer MoS_2, Mo and S atomic potentials overlap along the projection direction, resulting in almost equal intensities in all the atomic columns. Whereas for monolayer, the intensity line trace shows higher signal from Mo atoms compared to S atoms under negative C_S imaging condition (Fig. 2(b)), and this is because of higher atomic number of Mo (42) compared to S (16).[1,28] MoS_2 shows regular hexagonal diffractogram or Fourier transform (FT) corresponding to 2H structure (inset FT of Fig. 2(b)), where in projection image three S atoms will appear surrounding one Mo atom. It was reported previously that for Li intercalated MoS_2 the structure is stabilized to the metastable 1T poly-type and can exhibit different metastable superstructures, e.g., $\sqrt{3}a \times a$ or $2a \times a$, $\sqrt{3}a \times \sqrt{3}a$ or $2\sqrt{3}a \times 2\sqrt{3}a$ due to two dimensional Peierls distortions.[7,28,29] However, no such superstructures are observed either by imaging or diffraction in the present MoS_2 sample. In ReS_2, the most stable structure is Peierls distorted $1T_d$ associated with the periodic modulation, involving clustering of four Re atoms forming a Re_4 "diamond unit" and coupling between such units give rise

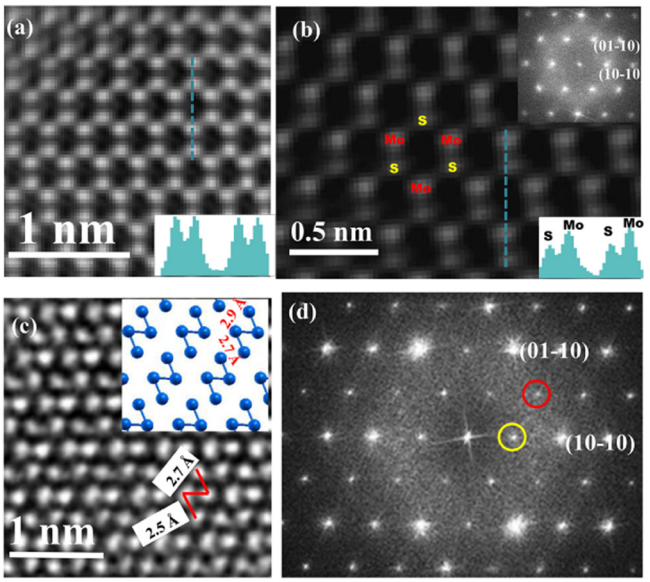

FIG. 2. HRTEM images of (a) multilayer 2H-MoS_2 along ⟨0001⟩. The intensity profile across the columns is shown in the lower right inset, the intensity from Mo and S columns is almost same in this case. (b) Monolayer 2H-MoS_2. Mo and S atoms are marked. The diffractogram or FT is shown in the upper right inset, the intensity profile across the columns is shown in the lower right inset, and the intensity line trace gives higher signal for Mo compared to S. HRTEM of (c) monolayer distorted 1T-ReS_2. The "N" shaped Re_4 cluster is highlighted. The DFT calculated Re_4 clusters are shown in the upper right inset. (d) FT of distorted 1T-ReS_2. The superstructure spots are marked with the yellow circles.

to "diamond chains" (Fig. 2(c)). This distortion has its origin in minimization of the energy of electrons by opening a gap at half way in the Brillouin zone due to the presence of large number of states at the E_F, and the resulting gain in energy is more than the elastic energy cost on the formation of Re_4 diamond unit.[11,30] The dimensions as indicated in Fig. 2(c) of the Re_4 clusters are measured to be 2.5 Å/2.7 Å and 2.7 Å/2.9 Å from atomic resolution imaging and DFT calculation, respectively. The (10-10) and (01-10) diffraction spots are marked in the FT of ReS_2 HRTEM image (Fig. 2(d)). The diffractogram of $1T_d$ structure is different than 2H counterpart with extra spots appearing along ⟨11-20⟩ due to rotation of one of the S hexagons by 30° with respect to rest of the hexagons corresponding to Re and S atoms in a unit cell.[28] The superstructure spots corresponding to the Re_4 clusters are marked with the yellow circles having periodicity of $g = \frac{1}{2}\langle 01\text{–}10\rangle$.

B. Layer specific band gap measurement by HREELS

The unique advantage of EELS in a TEM is that it is possible to select layer specific areas, and the band gap measurement can be performed with high spatial resolution. This technique has the added benefit that one single TEM sample grid can provide many different layer specific areas. In the mono probe mode, a very small area $\sim 5\,nm^2$ can be selected by appropriate combination of objective magnification and slit width at the height of the C1 lens, and condenser lens can further be used to de-magnifying the mono probe on the specimen in order to compensate the signal loss at higher magnification.[31–33] GIF entrance aperture can further be used as a selected area aperture to select very small area through which signal is finally fed into the spectrometer.

C. Calculated electronic structure, corresponding optical response, and Tauc plots

We begin with the theoretical description of optical response and corresponding electronic structures of both MoS_2 and ReS_2 in comparison to ZnO because of significant difference between the two systems in terms of dimensionality of covalent chemical bonding, i.e., 2D (van der Waals along the third dimension) *vs.* 3D and thus applicability of Tauc plot in determining the type of band gaps and values. Previously, a step function like fitting along with joint density of states (JDOS) for direct band gap and phonon assisted absorption function for indirect band gap was used for MoS_2, which is similar to the ideal 2D electron gas problem where DOS is typically independent of energy.[2] However, in quasi 2D systems like MoS_2 and ReS_2, the DOS is not energy independent, has a specific structure, and the analysis of absorption spectra may be complicated. Though Tauc plot works well for ZnO like systems where the bands are parabolic for a wide energy range and reciprocal momentum vectors, no competing transition events appear till ∼5 eV from the VBM, and no significant Van Hove singularities are present in DOS till 4 eV from the onset of transition.[33] Under such scenario, both energy loss function and Tauc plot ($(\alpha.E)^2$ *vs.* E) yield easy detection of band gap and its type, i.e., 3.3 eV and direct through linear extrapolation with large numbers of correlated data points.[33] Around 4 eV due to sharp feature in density of states in the valence band, the curve starts deviating from the linear behavior. If one plots $(\alpha.E)^{0.5}$ *vs.* E corresponding to indirect transitions, then one obtains a poor linear behavior at the onset and a feature at 3.3 eV is because of dominating direct transition. However, the scenario is complicated for MoS_2 where the parabola bands are shallow, and competing direct and indirect transition types are present within 0.5 eV of energy range and the DOS has sharp Van Hove singularities both at the VBM and CBM edges which will dominate the features both in the theoretical energy loss function and Tauc like plots. The difference between the theoretical and experimental energy loss function and the Tauc like plot is that the probability of transitions is selected phenomenologically for the latter case and helps finding the most probable direct or indirect band gap, whereas the theory calculations consider all possible transitions including phonon assisted inter-band transitions integrated over the Brillouin zone. However, if one of them is dominating, then the determination of another type of band gap becomes difficult through usual linear extrapolation if the energy difference is small. This is the case for MoS_2 bilayer but can be detected from the distinct features with the help of theory and is discussed further along with the experimental results in Sec. IV D. For ReS_2, such difficulty is not encountered as no such competing transitions are observed either theoretically or experimentally, though the bands are shallower. This is because of only one type of direct transitions present in this system.

As already reported previously,[34] for MoS_2, the VBM and the CBM at K point are made of Mo *d* states with subtle contribution from S p_z states (Figs. 3(a)–3(d)). Moreover, the CBM states at Λ point and the VBM states at Γ point are made of Mo *d* states hybridized with S p_z states. For monolayer, the VBM energy values are nearly same at K and Γ points, and the CBM at Λ point is slightly higher than at K point and the transition across K points becomes fundamental and direct (1.7 eV). When monolayers stack to form bulk MoS_2, the S p_z states get modified because of inter layer coupling interaction which leads to band renormalization, and the VBM states at Γ point shift higher in energy and the CBM states at Λ point shift lower in energy, resulting in indirect band gap (1.32 eV) as fundamental gap in bulk MoS_2. On the other hand, for distorted monolayer $1T_d$ ReS_2, the fundamental gap is across the Γ point where both Re *d* and S p_z states are hybridized (Figs. 3(e)–3(h)). Therefore, other than a slight decrease in band gap from 1.35 eV to 1.23 eV in the bulk, no change in the nature of band gap is observed in distorted $1T_d$ ReS_2.

Figs. 4(a) and 4(b) show the theoretical and experimental ELF of monolayer MoS_2, respectively. The spin-orbit split twin exciton peaks at the K point of the Brillouin zone are marked as A and B and experimentally appear at 1.8 and 1.95 eV, respectively. Similar experimental peak is observed based on optical absorption spectroscopy with a slight difference in the peak positions.[35] The difference in peak position between the theory (1.67 and 1.82 eV) and the experiment could be due to inaccuracy in calculating exact form of the excited states in the system. The three transitions peaks A, B, and C identified in both the theoretical and experimental energy loss function of monolayer MoS_2 have been

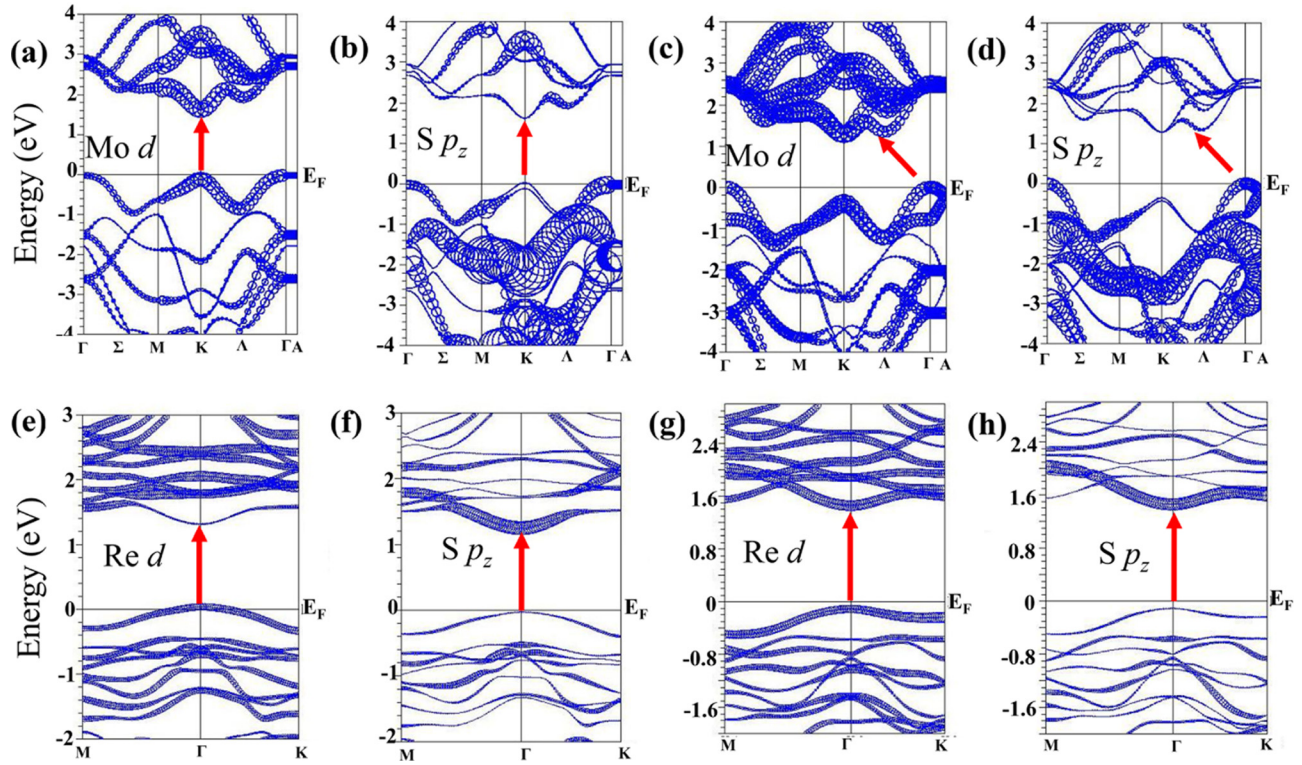

FIG. 3. Band character plots of Mo *d* and S p_z in (a) and (b) monolayer 2H-MoS_2 and (c) and (d) bulk 2H-MoS_2, respectively. The same for (e) and (f) monolayer distorted 1T-ReS_2 and (g) and (h) multilayer distorted 1T-ReS_2. The weight of the density of states at different momentum points is also shown.

correlated with the corresponding DOS plot (Fig. 4(c)). Peaks A and B at the onset in the energy loss function are the spin orbit split d_Z^2 *to* d_Z^2* (VBM to CBM) transitions. The peak at 3 eV corresponds to Mo d_Z^2 to Mo $d_{x^2-y^2}$ transition. Note that the $\Delta l \neq 1$ transitions are allowed because of hybridization between the states. The ELF along with DOS for bulk MoS_2 is shown in Figs. 4(d)–4(f). Peak A′ at the onset and peak B′ at 3 eV are marked and have the same origin as mentioned above.

Now the theoretical Tauc like plots corresponding to both direct and indirect transitions for both monolayer and bulk MoS_2 are shown in Figs. 5(a) and 5(b). Only high intensity plots of ELF and absorption coefficient corresponding to *xx* and *yy* are considered for the discussion, *zz* are shown only for the purpose of reference. The appearance of ELFs is almost similar between the monolayer and the bulk but there are subtle differences which help to identify the types and values of band gaps. From Fig. 5(b), the twin excitonic peaks at 1.67 and 1.82 eV can be identified. From Fig. 5(b), it is not possible to identify indirect transitions as the plot is dominated by direct band gap at the onset. The twin excitonic peak can be observed in both the Tauc like plots. The Tauc like plots for bulk MoS_2 look similar (Figs. 5(c) and 5(d)), but there are no data points through which a linear

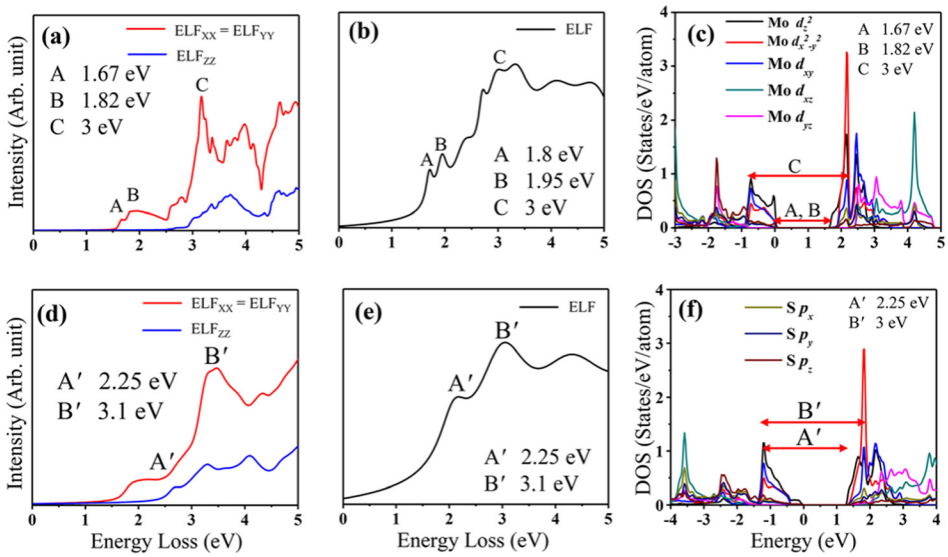

FIG. 4. (a) and (d) Theoretical, (b) and (e) experimental energy loss functions, and (c) and (f) DOS for monolayer and bulk 2H-MoS_2, respectively. The transitions associated with sharp features are marked and correlated with DOS.

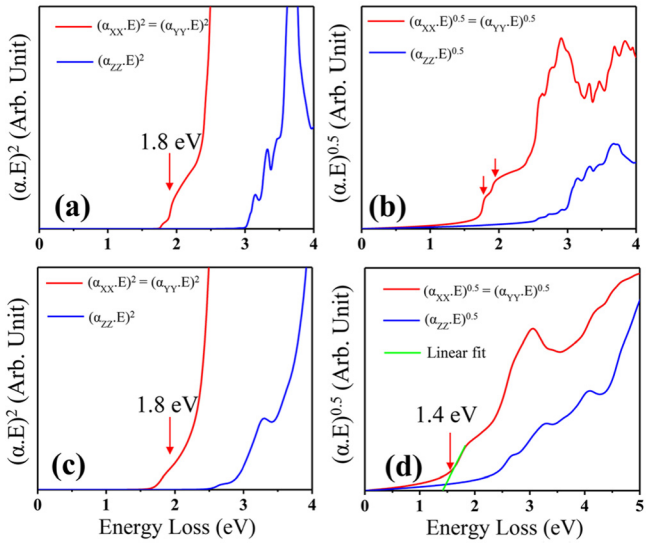

FIG. 5. Tauc plots corresponding to determination of direct and indirect band gaps for (a) and (b) monolayer and (c) and (d) multilayer MoS_2, respectively. The twin exciton peaks are marked for the monolayer. The peak related to direct band gap for bulk is also marked.

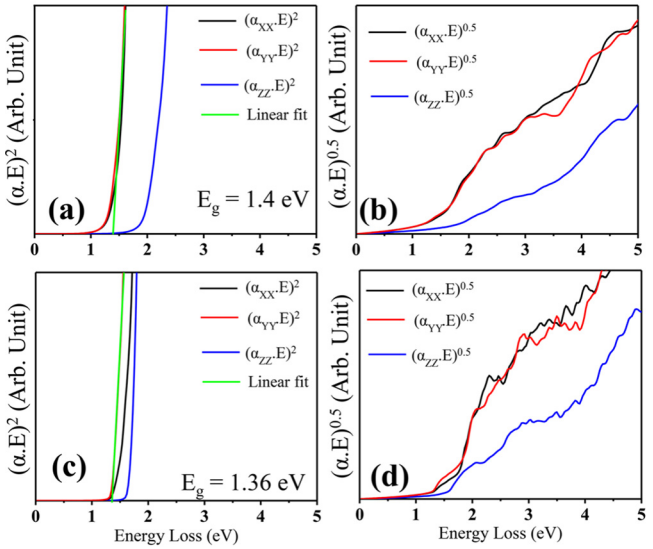

FIG. 7. Tauc plots corresponding to determination of direct and indirect band gaps for (a) and (b) distorted monolayer and (c) and (d) multilayer 1T-ReS_2.

fit can be made except at 1.4 eV which corresponds to the indirect transitions. The feature at 1.8 eV is because of direct band gap transitions in both the Tauc like plots. The excitonic peaks are not observed in this case as spin orbit splitting is absent in bulk MoS_2 due to the presence of inversion symmetry and comparative one order of magnitude lower exciton binding energy (0.1 eV).[10] From the equivalent experimental plot, we will observe further differences as relative probability of competing transitions is not taken into account in the theoretical calculations, whereas in the experimental spectra it is selected phenomenologically.

The theoretical and experimental ELF for monolayer distorted $1T_d$ ReS_2 is shown in Figs. 6(a) and 6(b). The peaks at 2 and 3 eV (A and B) are indicated. Peak A is the transition from d_{yz} to d_{x2-y2}*. Peak B is due to d_z^2 to d_z^2* transition (Fig. 6(c)). After the onset, the ELF is flat because of almost flat *p-d* hybridized bands on both sides of the Fermi level and the presence of states at higher energy range. Figs. 6(d) and 6(e) show the ELF from multilayer distorted $1T_d$ ReS_2. It shows rather abrupt onset and can be explained by the steep valence band offset and conduction band onset of DOS compared to monolayer. After the onset, the ELF in this case is also flat because of delocalized *d* state hybridized with S-*p* states forming flat DOS on both sides of the Fermi energy (Fig. 6(f)). The theoretical Tauc like plots corresponding to both direct and indirect band gaps for monolayer and bulk ReS_2 are shown in Fig. 7. In this case, the onset gives a clear identification of direct band gap type, and the plot for indirect band gap is poorly linear. This is because of non existence of competing transitions unlike MoS_2.

We would like to elaborate on the electronic structure of Peierls distorted $1T_d$ ReS_2. The band structure and the DOS of undistorted $1T_d$-ReS_2 are given in Fig. S2(b) of supplementary

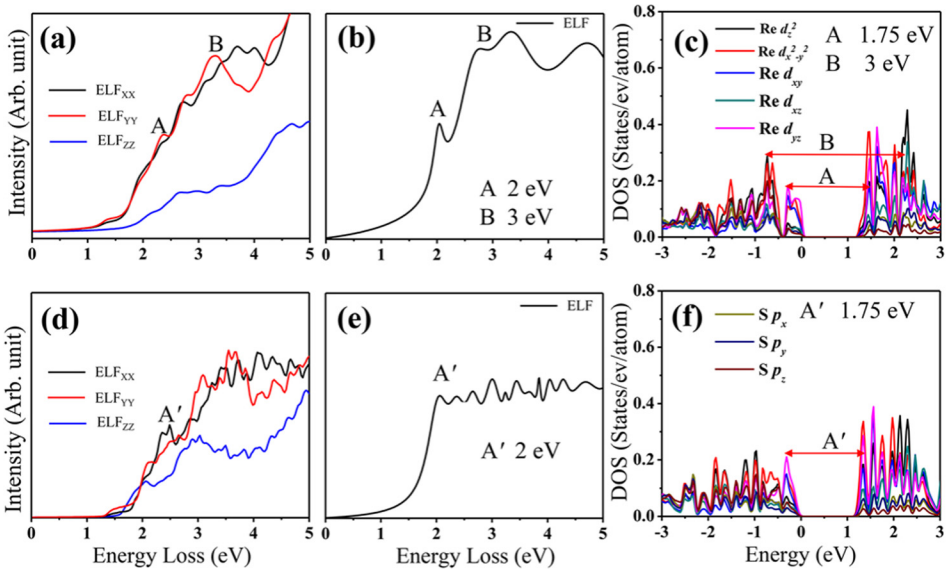

FIG. 6. (a) and (d) Theoretical, (b) and (e) experimental energy loss functions, and (c) and (f) DOS for distorted monolayer and bulk 1T-ReS_2, respectively. The transitions associated with sharp features are marked and correlated with DOS.

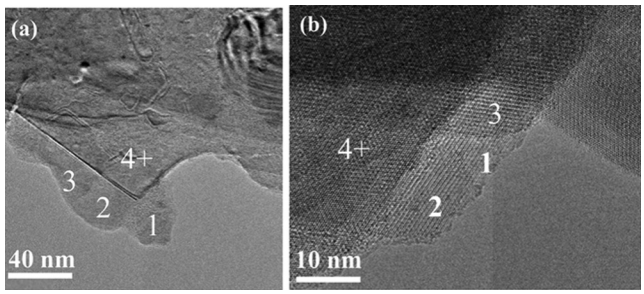

FIG. 8. Example low magnification image from (a) MoS_2 and (b) ReS_2 showing different number of layers used for the experimental band gap study. Fresnel contrast at the edge helps identifying number of layers.

material.[31] In $1T_d$-ReS_2, Re is in a d^3 electron configuration. The lower energy t_{2g} states are half filled resulting in Peierls instability. In distorted $1T_d$ ReS_2, the hybridization between Re d and S p orbitals is similar to undistorted $1T_d$ ReS_2, but in the latter case, the Re atoms form Re_4 clusters to form a 2×2 superstructure. A band gap is formed exactly at the Fermi level which was in the middle of the half-filled t_{2g} states. This structural reconfiguration takes place (Peierls distortion), because the gain in energy due to opening a band gap is higher than the elastic energy due to formation of Re_4 cluster. The distorted $1T_d$ ReS_2 is more stable by 563 meV and 315 meV than undistorted $1T_d$ and 2H ReS_2, respectively. The anisotropic electronic structure of ReS_2 can be engineered by the application of strain along different directions with respect to the Re_4 diamond chain.[30,36] It was also reported that the formation of S vacancy is energetically favorable in this system and the formation of Re vacancy gives rise to magnetism.[37] The anisotropic absorption obtained by experiment in this system is in the range of 0.05 eV (Ref. 38) and 0.025 eV with respect to the axis system used in this manuscript, which is consistent in terms of no significant difference in the absorption onset of ELF calculated in the present report but differs largely with the theoretical calculation reported in Ref. 35.

D. Layer specific band gap measurement of MoS_2 and ReS_2 by HREELS

Figs. 8(a) and 8(b) show the example low magnification image of MoS_2 and ReS_2 with different number of layers' areas is marked accordingly. The band gap values have been extracted from the Tauc like plot corresponding to direct $((\alpha.E)^2$ *vs.* E) and indirect $((\alpha.E)^{0.5}$ *vs.* E) band gaps. Example of such plots for monolayer and multilayer MoS_2 is given in Figs. 9(a)–9(d). The Tauc like plot for direct band gap $((\alpha.E)^2$ *vs.* E) shows a sharp onset (Fig. 9(a)). A direct band gap value of 1.98 eV is obtained for the monolayer. The Tauc like plot corresponding to indirect band gap shows a poor linear behavior owing to the absence of any significant phonon assisted transition in monolayer MoS_2 and is in contrast with the theoretical calculation, which considers this transition probability in the calculation. The twin exciton peaks at 1.8 and 1.95 eV are only visible in the experimental energy loss function (Fig. 4(b)) and are smeared out in the Tauc like plot. The exciton binding energy is reported to be very high, i.e., 1.1 eV in monolayer MoS_2, thus can be observed even in a room temperature measurement.[10] The exciton wave function extent is nearly 7 nm for MoS_2.[39] The excitons have been previously measured in the STEM mode with very low beam voltage (30 kV), more sensitive Gatan Quantum spectrometer, ultra high energy resolution (20–36 meV), and after cooling the sample at about 150 K. But we have been able to measure the exciton in the parallel beam mode (5 sq nm spatial resolution), operating at 300 kV beam energy with a Gatan Tridiem spectrometer, at room temperature, and with a one order of magnitude inferior energy resolution (180 meV). Therefore, our results suggest that the present gun monochromator system can still be used for studying strongly bound excitons at the nanometer length scale.

Fig. 9(d) is the Tauc plot for indirect band gap and shows a steep linear behavior. An indirect band gap value of 1.27 eV has been obtained which is very close to the band

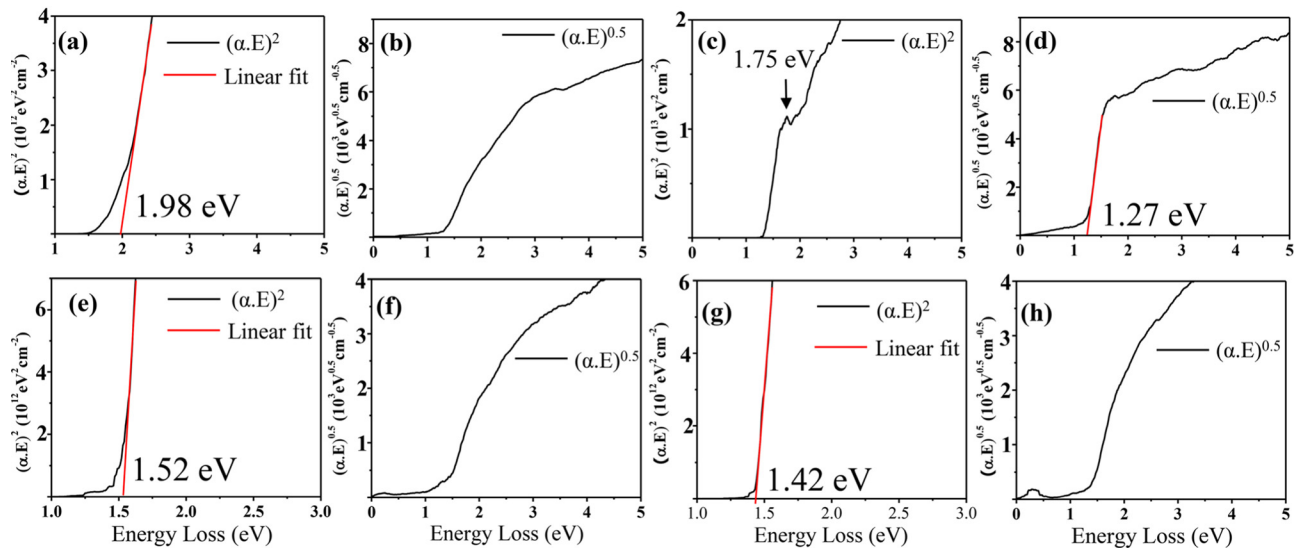

FIG. 9. Example experimental Tauc plots corresponding to direct and indirect band gaps for (a) and (b) monolayer MoS_2, (c) and (d) multilayer MoS_2, (e) and (f) monolayer ReS_2, and (g) and (h) multilayer ReS_2, respectively.

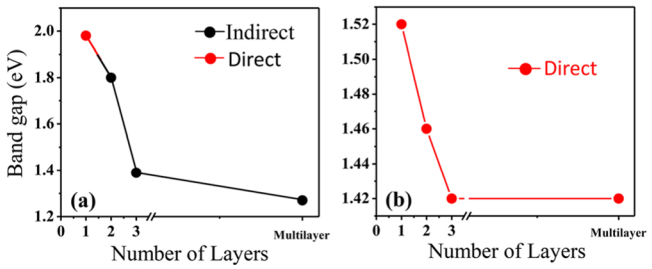

FIG. 10. Layer specific plots of band gaps and their types for (a) MoS_2 and (b) ReS_2. Note the direct to indirect band gap crossover for MoS_2 from monolayer to bilayers.

gap (1.29 eV) found for bulk MoS_2.[2,40] However, the Tauc like plot for direct band gap (Fig. 9(c)) is dominated by indirect transitions, and only the direct transition peak can be identified at 1.75 eV. This occurs because of two different transitions having almost similar probability unlike in the case of monolayer where only direct transition is significant. This is probably due to the significant difference in exciton binding energy between the monolayer (1.1 eV) and the bulk (0.1 eV). From bilayers' and three layers' region, an indirect band gap of 1.8 and 1.39 eV is obtained, respectively.

The Tauc plots for monolayer and multilayer ReS_2 are given in Figs. 9(e)–9(h). For multilayer, the Tauc like plot for indirect band gap does not show any linear segment, while the Tauc like plot for direct band gap gives a value of 1.42 eV. For monolayer, the Tauc plots show similar behavior, and a direct band gap of 1.52 eV is obtained (Fig. 9(e)). It was already reported that for ReS_2 both monolayer and many layers will show direct band gap due to weak interlayer coupling and van der Waals interaction. The EELS has the advantage in this case compared to the reported very broad PL emission from monolayer ReS_2 probably cross signals coming from neighboring regions with varying number of layers.[11] Finally, Fig. 10 plots the layer number dependent band gap values and the type for both MoS_2 and ReS_2. A direct to indirect crossover is observed for MoS_2, and for ReS_2 no such crossover is observed.

V. CONCLUSIONS

We have studied the layer specific optical band gaps at the nanoscale of mono to a few layers of 2H-MoS_2 and distorted 1T-ReS_2 by spatially resolved HREELS technique. An indirect band gap of 1.27 eV and a direct band gap of 1.98 eV are obtained for multilayer and monolayer MoS_2, respectively. The spin orbit split K-point exciton has been observed for the monolayer MoS_2. A direct to indirect band gap cross over is observed between monolayer to bilayer MoS_2. ReS_2 showed direct band gaps of 1.52 eV and 1.42 eV for mono and multilayer, respectively. The chemically synthesized 1T-ReS_2 is found to be in a Peierls distorted Re_4 cluster configuration. The results demonstrate the power of HR-EELS technique as a nanoscale optical absorption spectroscopy tool where no other alternative exists in terms of simultaneous imaging and spectroscopy at the atomic and nanometer length scale.

ACKNOWLEDGMENTS

The authors at JNCASR sincerely acknowledge Professor C. N. R. Rao for his constant support, and providing advanced transmission electron microcopy facility for this research.

[1]H. S. S. R. Matte, A. Gomathi, A. K. Manna, D. J. Late, R. Datta, S. K. Pati, and C. N. R. Rao, Angew. Chem., Int. Ed. **49**, 4059 (2010).
[2]K. Mak, C. Lee, J. Hone, J. Shan, and T. F. Heinz, Phys. Rev. Lett. **105**, 136805 (2010).
[3]A. Splendiani, L. Sun, Y. Zhang, T. Li, J. Kim, C.-Y. Chim, G. Galli, and F. Wang, Nano Lett. **10**, 1271 (2010).
[4]Q. H. Wang, K. Kalantar-Zadeh, A. Kis, J. N. Coleman, and M. S. Strano, Nat. Nano **7**, 699 (2012).
[5]M. M. Ugeda, A. J. Bradley, S. F. Shi, F. H. Jornada, Y. Zhang, D. Y. Qiu, W. Ruan, S. K. Mo, Z. Hussain, Z. X. Shen, F. Wang, S. G. Louie, and M. F. Crommie, Nat. Mat. **13**, 1091 (2014).
[6]D. Jariwala, V. K. Sangwan, L. J. Lauhon, T. J. Marks, and M. C. Hersam, ACS Nano **8**, 1102 (2014).
[7]S. N. Shirodhkar and U. V. Waghmare, Phys. Rev. Lett. **112**, 157601 (2014).
[8]B. Radisavljevic, A. Radenovic, J. Brivio, V. Giacometti, and A. Kis, Nat. Nanotechnol. **6**, 147 (2011).
[9]A. Kuc, N. Zibouche, and T. Heine, Phys. Rev. B **83**, 245213 (2011).
[10]H.-P. Komsa and A. V. Krasheninnikov, Phys. Rev. B **86**, 241201 (2012).
[11]S. Tongay, H. Sahin, C. Ko, A. Luce, W. Fan, K. Liu, J. Zhou, Y.-S. Huang, H. Ching-Hwa, J. Yan, D. F. Ogletree, S. Aloni, J. Ji, S. Li, J. Li, F. M. Peeters, and J. Wu, Nat. Commun. **5**, 3252 (2014).
[12]K. Dileep, B. Loukya, N. Pachauri, A. Gupta, and R. Datta, J. Appl. Phys. **116**, 103505 (2014).
[13]K. Dileep, B. Loukya, P. Silwal, A. Gupta, and R. Datta, J. Phys. D: Appl. Phys. **47**, 405001 (2014).
[14]O. L. Krivanek, T. C. Lovejoy, N. Dellby, T. Aoki, R. W. Carpenter, P. Rez, E. Soignard, J. Zhu, P. E. Batson, M. J. Lagos, R. F. Egerton, and P. A. Crozier, Nature **514**, 209 (2014).
[15]C. L. Jia, M. Lentzen, and K. Urban, Science **299**, 870 (2003).
[16]R. Datta, S. Kanuri, S. V. Karthik, D. Mazumdar, J. X. Ma, and A. Gupta, Appl. Phys. Lett. **97**, 071907 (2010).
[17]J. Tauc, Mater. Res. Bull. **3**, 37 (1968).
[18]M. S. Dresselhaus, *Solid State Physics Part II Optical Properties of Solids* (2001); available at http://web.mit.edu/course/6/6.732/www/6.732-pt2.pdf.
[19]J. I. Pankove, *Optical Process in Semiconductors* (Dover Books on Physics, 1971).
[20]P. Blaha, K. Schwarz, G. K. H. Madsen, D. Kvasnicka, and J. Luitz, *WIEN2k: An Augmented Plane Wave + Local Orbitals Program for Calculating Crystal Properties* (Karlheinz Schwarz, Techn. Universität Wien, Austria, 2001).
[21]S. Grimme, J. Antony, S. Ehrlich, and H. Krieg, J. Chem. Phys. **132**, 154104 (2010).
[22]A. Schindlmayr, Phys. Rev. B **87**, 075104 (2013).
[23]C. Friedrich, M. Betzinger, M. Schlipf, S. Blugel, and A. Schindlmayr, J. Phys.: Condens. Matter **24**, 293201 (2012).
[24]F. Tran and P. Blaha, Phys. Rev. Lett. **102**, 226401 (2009).
[25]D. Koller, F. Tran, and P. Blaha, Phys. Rev. B **85**, 155109 (2012).
[26]D. Koller, F. Tran, and P. Blaha, Phys. Rev. B **83**, 195134 (2011).
[27]C. Ambrosch-Draxl and J. O. Sofo, Comput. Phys. Commun. **175**, 1 (2006).
[28]U. Maitra, U. Gupta, M. De, R. Datta, A. Govindaraj, and C. N. R. Rao, Angew. Chem., Int. Ed. **52**, 13057 (2013).
[29]M. Chhowalla, H. S. Shin, G. Eda, L.-J. Li, K. P. Loh, and H. Zhang, Nat. Chem. **5**, 263 (2013).
[30]S. Yang, C. Wang, H. Sahin, H. Chen, Y. Li, S.-S. Li, A. Suslu, F. M. Peeters, Q. Liu, J. Li, and S. Tongay, Nano Lett. **15**, 1660 (2015).
[31]D. S. Negi, B. Loukya, K. Ramasamy, A. Gupta, and R. Datta, Appl. Phys. Lett. **106**, 182402 (2015).
[32]B. Loukya, X. Zhang, A. Gupta, and R. Datta, J. Magn. Magn. Mater. **324**, 3754–3761 (2012).
[33]See supplementary material at http://dx.doi.org/10.1063/1.4944431 for details of HREELS experiment, band gap measurement of two layers and three layers MoS_2 and ReS_2, and the electronic structure of ZnO.
[34]X. B. Chen, Z. L. Chen, and L. Jun, Chin. Sci. Bull. **58**, 1632 (2013).
[35]J. N. Coleman, M. Lotya, A. O'Neill, S. D. Bergin, P. J. King, U. Khan, K. Young, A. Gaucher, S. De, R. J. Smith, I. V. Shvets, S. K. Arora, G. Stanton, H. Y. Kim, K. Lee, G. T. Kim, G. S. Duesberg, T. Hallam, J. J. Boland, J. J. Wang, J. F. Donegan, J. C. Grunlan, G. Moriarty, A.

Shmeliov, R. J. Nicholls, J. M. Perkin, E. M. Grieveson, K. Theuwissen, D. W. McComb, P. D. Nellist, and V. Nicolosi, Science **331**, 568 (2011).
[36]H.-X. Zhong, S. Gao, J.-J. Shi, and L. Yang, Phys. Rev. B **92**, 115438 (2015).
[37]S. Horzum, D. Çakır, J. Suh, S. Tongay, Y.-S. Huang, C.-H. Ho, J. Wu, H. Sahin, and F. M. Peeters, Phys. Rev. B **89**, 155433 (2014).
[38]C.-H. Ho, Cryst. Struct. Theory Appl. **2**, 65 (2013).
[39]L. H. G. Tizei, Y.-C. Lin, M. Mukai, H. Sawada, A.-Y. Lu, L.-J. Li, K. Kimoto, and K. Suenaga, Phys. Rev. Lett. **114**, 107601 (2015).
[40]L. Gmelin, *Gmelin Handbook of Inorganic and Organometallic Chemistry* (Springer-Verlag, Berlin, 1995).